J Seismol
DOI 10.1007/s10950-012-9331-6

ORIGINAL ARTICLE

The January 2010 Efpalion earthquakes (Gulf of Corinth, Central Greece): earthquake interactions and blind normal faulting

Athanassios Ganas · Kostas Chousianitis · Evaggelia Batsi · Maria Kolligri · Apostolos Agalos · Gerassimos Chouliaras · Kostas Makropoulos

Received: 8 August 2011 / Accepted: 29 August 2012

Abstract On 18 January 2010, 15:56 UTC, a M_w=5.1 (National Observatory of Athens; NOA) earthquake occurred near the town of Efpalion (western Gulf of Corinth, Greece), about 10 km to the east of Nafpaktos, along the north coast of the Gulf. Another strong event occurred on 22 January 2010, 00:46 UTC with M_w=5.1 (NOA) approximately 3 km to the NE of the first event. We processed the seismological and geodetic data to examine fault plane geometry, dip direction, and earthquake interactions at the western tip of the Corinth rift. Our data include relocated epicenters of 1,760 events for the period January–June 2010 and daily global positioning system observations from the Efpalio station for the period 1 December 2009–1 March 2010. We suggest that the first event ruptured a blind, north-dipping fault, accommodating north–south extension of the Western Gulf of Corinth. The dip direction of the second event is rather unclear, although a south dip plane is weakly imaged in the post-22 January 2010 aftershock distribution. A Coulomb stress model based on homogeneous slip distribution of the first event showed static stress triggering of the second event of the order of 22–34 KPa that was transferred along the plane of failure. We also point out the existence of north dipping, high-angle faults at 10–15 km depths, which were reactivated because of Coulomb stress transfer, to the west and south of Efpalion. The January 2010 earthquakes ended a 15-year-old quiescence in that area of the Gulf. The crustal volume near Efpalion was also characterized by *b* values in the range 0.6–0.8 (1970–2010 period).

Keywords Earthquake interaction · Normal faulting · HypoDD · GPS · Corinth · Greece

A. Ganas (✉) · K. Chousianitis · E. Batsi · M. Kolligri · A. Agalos · G. Chouliaras · K. Makropoulos
Institute of Geodynamics, National Observatory of Athens, 11810 Athens, Greece
e-mail: aganas@gein.noa.gr

1 Introduction

On 18 January 2010, 15:56 UTC, a M_w=5.1 (National Observatory of Athens; NOA) moderate earthquake occurred near the town of Efpalion, about 10 km to the east of Nafpaktos, along the north coast of the Gulf of Corinth (Fig. 1, yellow stars). On 22 January 2010, 00:46 UTC, a second event of M_w=5.1 (NOA) occurred a few kilometers to the east of 18 January 2010 event. No casualties or serious damage was reported. Focal mechanism solutions by Sokos et al. (2012) determined east–west striking fault planes with a dominant component of normal slip (strike/dip/rake 102°/55°/−83° and 270°/36°/−100° for the first event; 282°/52°/−75° and 78°/40°/−109° for the second event). This sequence ended a 15-year seismic quiescence in this area of Greece as the last major event was the Aigion (June 1995, M_S=6.2), offshore earthquake about 20 km to the east of Efpalion (Bernard et al. 1997; event 061595A in Fig. 1).

The Efpalion area occupies the north coast of the Gulf of Corinth and comprises Mesozoic–Early Tertiary sedimentary rocks of the so-called External Hellenides tectonic nappes. The thrusts are west verging and of

Published online: 06 October 2012

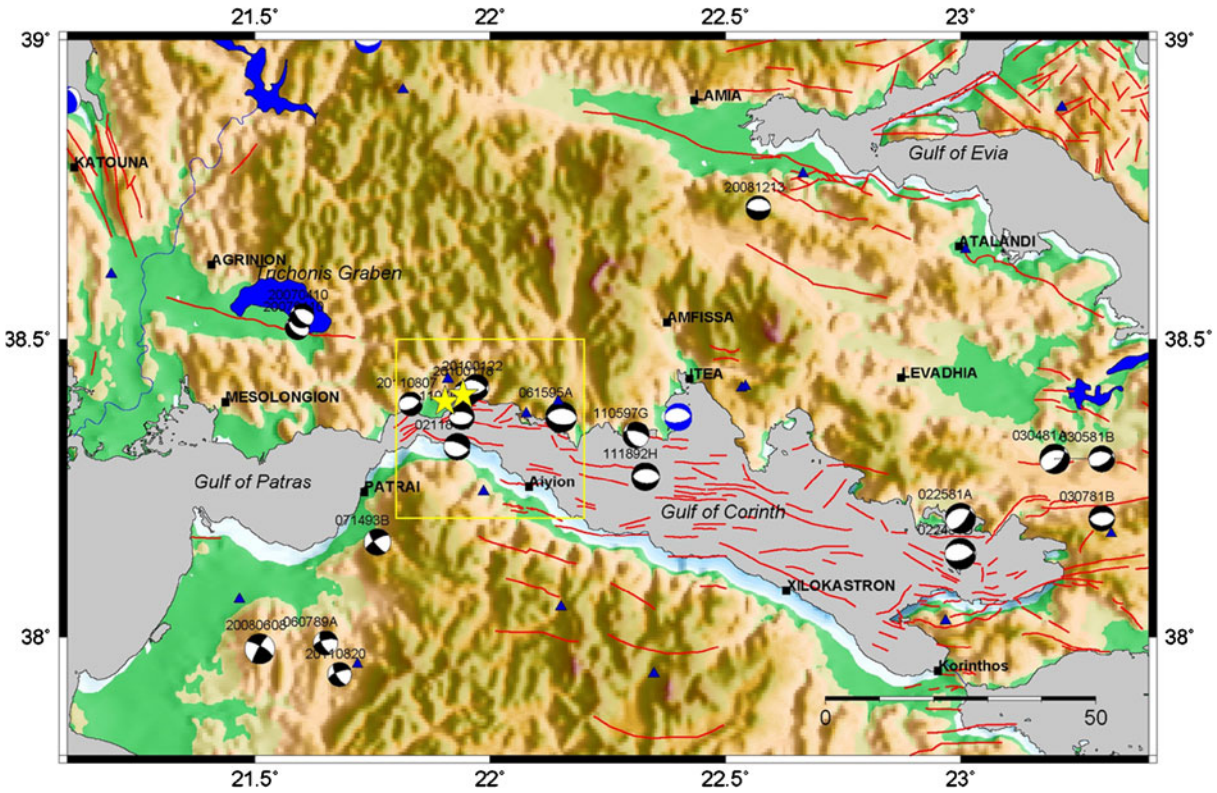

Fig. 1 Relief map of Central Greece showing focal mechanisms of strong, shallow events since 1977 (Global CMT catalog). *Yellow stars* are the Efpalion earthquakes of January 2010. *Blue triangles* are broadband seismic stations of HUSN used in relocation. *Thin red lines* are active faults. The January 2010 earthquakes ended a 15-year-old quiescence in that area. *Box* shows area of Fig. 3

Late Eocene–Oligocene Age. The main structural feature is the contact between the shallow Parnassus unit and the abyssal Pindos unit (Doutsos et al. 2006). Nappe stacking and crustal shortening during most of Tertiary led to formation of thick crust. In particular, the thickness of the continental crust in this area is the highest of central Greece, 40 km (Zelt et al. 2005).

Since Pliocene, this region is one of the most active extensional continental regions in the world, located between the two lithospheric plates of Eurasia and Africa, which converge at a combined rate of about 3–4 cm/year. The geological evidence of normal faulting and the high seismicity, both historical and instrumental, imply a high rate of extension. In particular, the western Gulf of Corinth is a young (Quaternary) graben characterized by fast extension rates (>1.5 cm/year; Briole et al. 2000; Avallone et al. 2004) and high seismicity (e.g., Rigo et al. 1996; Rietbrock et al. 1996; Hatzfeld et al. 1996; Jansky et al. 2004). The last major seismic event occurred on 15 June 1995 at 00:15 UTC when a M_S=6.2 earthquake rupture a low-angle fault offshore Aigion (Fig. 1; Bernard et al. 1997). After the 1995 event, the area was recognized as a site of global tectonic significance where a number of EU research projects have been completed (3F-Corinth, DG-Lab, CRL, CORSEIS, and several others are ongoing (see http://crlab.eu/ for a summary of research activity)). The overall concept of those research projects was that to move progressively towards a research infrastructure for the assessment of the seismic risk in the Gulf of Corinth region and to better understand the role of fluids and stress transfer in the crust and lithosphere and their role in the triggering of earthquakes. Recently, the Gulf of Corinth is included in the list of European Space Agency–Group on Earth Observation supersites (http://supersites.unavco.org/main.php).

Seismic activity inside the Gulf of Corinth was moderate to high following the June 1995 event, with no events with M>6 occurring inside the Gulf (Fig. 1). During the last 17 years (1995–2012), two shallow seismic sequences have occurred in the vicinity of the western Gulf of

Corinth (Fig. 1): (a) the April 2007 earthquake swarm at the eastern end of Trichonis Lake (three events with M=5.0–5.2, Kiratzi et al. 2008) and (b) the 8 June 2008 Movri mountain event in south Achaia (M=6.4, Ganas et al. 2009; Gallovic et al. 2009; Koukouvelas et al. 2009). In addition, a M_w=5.0 event occurred on 13 December 2008, near Amfiklia, Central Greece (Chouliaras 2009a, b; Roumelioti and Kiratzi 2008; event 20081213 in Fig. 1).

This paper presents (a) an analysis of seismological data collected by NOA (we gathered 1,760 earthquakes, including the two main seismic events, during the period 18 January–30 June 2010), (b) static processing results from global positioning system (GPS) observations, and (c) results from an earthquake-triggering model (based on static stress transfer) for this sequence. The main points of our findings was to identify the north-dipping plane as the 18 January 2010 slip plane and confirm the existence of north dipping, high-angle faults at 10–15 km depths, which were reactivated because of Coulomb stress transfer, to the west and south of Efpalion. These observations confirm the normal character of earthquake slip to the west of Aigion 1995 earthquake. An additional point is the recognition of nonspatial decay of earthquake magnitude during the early aftershock sequence (18–22 January 2010).

2 Data analysis

2.1 Seismic data

The location parameters of the two main shocks are reported in Table 1. The first, main seismic event occurred on 18 January 2010, with a local magnitude M_L=5.2 (M_w=5.1). It was followed by a second major seismic event at 22 January 2010, with a local magnitude M_L=5.1 (M_w=5.1). We relocated the epicenter of the 18 January 2010 as 38.3962° north, 21.9039° south, with depth of 8.5 km, while the epicenter of the 22 January 2010 is to the NE of the 18 January 2010 and shallower, i.e., 38.4075° north, 21.9422° south, depth of 5.1 km (Fig. 1). All earthquakes were relocated using the HYPOINVERSE (Y2000 version; Klein 2002) and the HYPODD (double difference; Waldhauser 2001) algorithms, in succession. Phase data were available from the permanent seismic network of NOA in HYPO71 (Lee and Lahr 1972) format.

For the region of our interest, we gathered 1,892 earthquakes, including the two main seismic events, during the period 18 January–30 June 2010. The parameters of these earthquakes were initially determined by the algorithm HYPO71, using the 1-D NOA velocity model (Table 2; Fig. 2). V_p/V_s ratio value used was 1.78. Next step was the relocation of all seismic events with the algorithm HYPOINVERSE. During this procedure, no data were

Table 1 Summary of location parameters for the Efpalio events as reported on the Internet

Organization	Date	Origin time	Latitude	Longitude	Depth	Magnitude
EMSC	18 January 2010	15:56:09.8	38.39	21.95	5	M_w=5.3
	22 January 2010	00:46:57.3	38.42	22.04	2	M_b=5.3
NOA catalog	18 January 2010	15:56:09.20	38.41	21.95	20	M_L=5.2
NOA MT	18 January 2010	15:56:12.00	38.48	22.00	5	M_w=5.1
NOA catalog	22 January 2010	00:46:56.20	38.42	21.97	12	M_L=5.1
NOA MT	22 January 2010	00:46:57.00	38.44	21.98	6	M_w=5.1
USGS (PDE)	18 January 2010	15:56:09.00	38.40	21.96	0	M_w=5.5
	22 January 2010	00:46:56.70	38.42	22.04	5	M_w=5.2
RCMT	18 January 2010	15:56:15.5	38.32	21.84	12	M_w=5.5
	22 January 2010	00:46:59.8	38.25	21.83	13	M_w=5.4
GLOBAL CMT	18 January 2010	15:56:13.7	38.34	22.02	13.5	M_w=5.5
This study	18 January 2010	15:56:09.60	38.3962	21.9039	8.5	M_L=5.2
	22 January 2010	00:46:56.47	38.4075	21.9422	5.1	M_L=5.1

Depth is in kilometer

MT seismic moment tensor, *NOA* National Observatory of Athens, *USGS* United States Geological Survey, *EMSC* Euro-Mediterranean Seismological Centre

Table 2 1-D velocity models used in relocation

NOA velocity model		Patras velocity model	
Depth (km)	V_p (km/s)	Depth (km)	V_p (km/s)
0.0	5.3	0.0	5.7
4.0	6.0	5.0	6.0
33.0	6.9	18.0	6.4
45.0	7.9	39.0	7.9
85.0	8.3		

rejected. The main characteristic of HYPOINVERSE that we exploited was that every phase (P and S) is assigned a weight code that indicates the weight that the phase carries to the final solution. After this relocation, considerable changes were observed in the epicenters and the depths of the 1,892 events, therefore, we continue with final part of our project, relocation of the seismic events using the HYPODD algorithm (double-difference earthquake algorithm). The double-difference technique allows the use of any combination of ordinary phase picks from earthquake catalogs and/or high-precision differential travel times from phase correction of P and/or S waves (cross-correlation data). We only have phase picks available from the earthquake catalogs of the National Observatory of Athens. Earthquake relocation with HYPODD is a two-step process. The first step involves the analysis of catalog phase data and/or waveform data to derive travel time differences for pairs of earthquakes. Processing of catalog phase data is done by using the *ph2dt* procedure.

In the second step, the differential travel time data from step 1 is used to determine double-difference hypocenter locations. This process is carried out by the hypoDD algorithm. For the area of our interest, we have chosen the conjugate gradients method (sparse equations and least squares; Paige and Saunders 1982) and the 1-D velocity model of Tselentis and Zahradnik (2000; referred

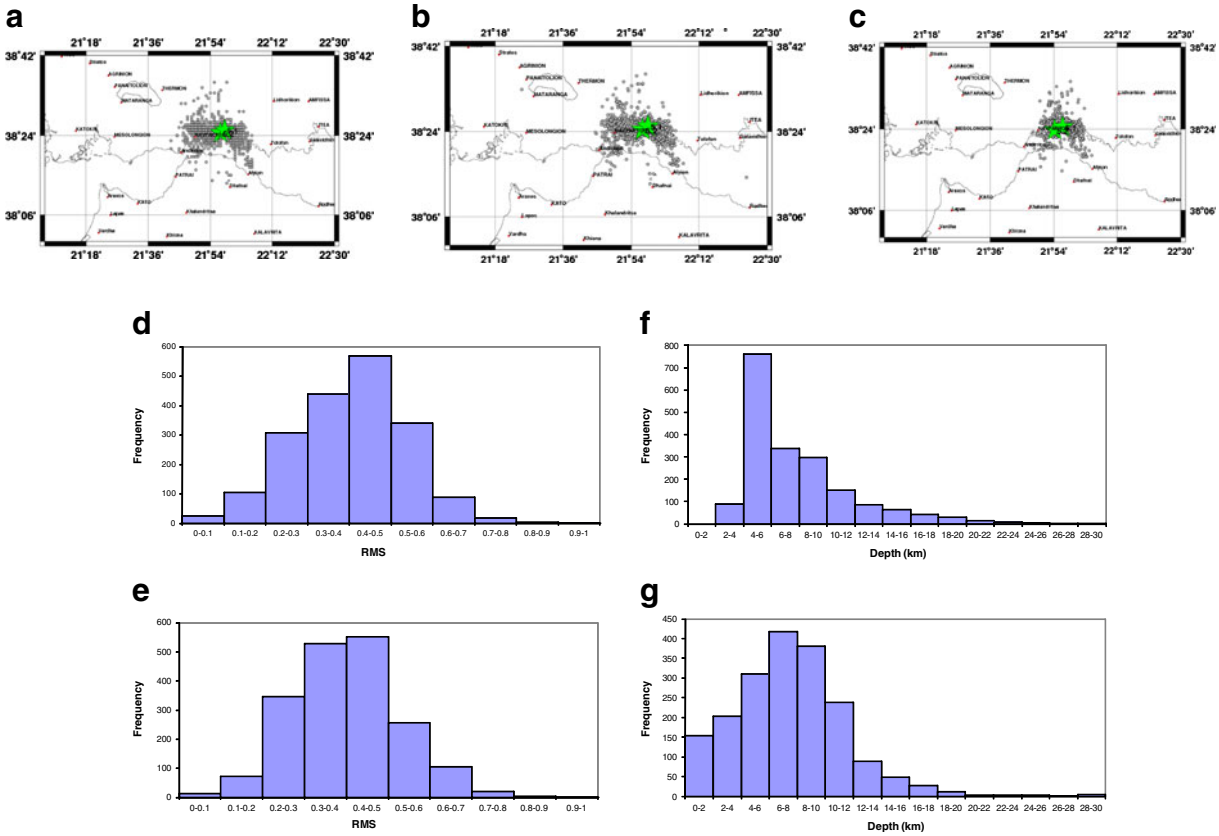

Fig. 2 **a–c** seismicity maps of Efpalio sequence representing successive steps in relocation procedure (Hypo71, Hypoinverse, HypoDD) as described in text. **d**, **e** Solution RMS error histograms (in seconds) for Hypo71 and Hypoinverse, respectively. **f**, **g** Hypocenter depth histograms (in km) for Hypo71 and Hypoinverse, respectively

as Patras model in brief, Table 2). We also tried the velocity models by Latorre et al. (2004) and Rigo et al. (1996) without significant changes in seismicity patterns, so we adopted the so-called Patras velocity model. An important parameter in the hypoDD algorithm which defines the clustering is the OBSCT parameter. This parameter defines the minimum number of catalog links that must be present to form a continuous chain needed to identify a cluster. In our case, we chose OBSCT=8, which is a typical choice, since it coincides with the number of degrees of freedom for an event pair (three spatial and one time for each event). In the earthquake sequence of 18 January 2010, from the 1,892 earthquakes, relocated by HYPOINVERSE, the 1,867 events were selected by the HYPODD algorithm and 63 stations from the Hellenic Unified Seismological Network (HUSN). The rest of the available stations were rejected since they were considered to be much distanced from the region of our study. This selection is defined by the parameters of the hypoDD algorithm, such as DIST, which shows the maximum distance between centroids of event clusters and stations. We chose DIST=380 km and we found that a unique cluster was formed, including 1,833 seismic events. The rest, 34 events, were considered as isolated events. By the end of the relocation (Fig. 2), the hypoDD algorithm concluded to 1,760 earthquakes and 63 contributing stations. The rejected events were due to reweighting or some events becoming airquakes.

Two hundred fifty-nine events occurred between 18 January 2010 (15:56 UTC) and 22 January 2010 (00:46 UTC) with 1.9<M<4.0. The map and cross-sections in Fig. 3a show the tight distribution of the seismic sequence in space during the first 3.5 days (Fig. 3a). Almost all aftershocks occur to the north and east of the 18 January 2010 main shock at depths of 4–12 km. The pattern of aftershock distribution in map view supports a north-dipping fault (nodal plane with strike/dip/rake 270°/36°/−100°) of Sokos et al. (2012), as it is common in normal-fault earthquakes that most aftershocks occur inside the hanging wall area for example, the 1999 Athens earthquake, (Baumont et al. 2004) and the 2009 L'Aquila earthquake (Chiarabba et al. 2009). The biggest cluster of aftershocks occurred in the hypocentral region of the 22 January 2010 event. This cluster exhibits a vertical structure (looking across strike) which suggests that the aftershocks occur within a highly stressed area to the east of the 18 January 2010 event and not along a particular fault plane. Plotting the entire seismicity (January–June 2010; Fig. 3b), it is seen that earthquakes occurred more to the east than to the west. In addition, the pattern of the 5-month seismicity has a clear east–west orientation, along the north coast of the Gulf of Corinth, which is a result of Coulomb stress loading in this orientation as we show later in this paper. Seismicity cross-sections also show a depth distribution of hypocenters from 4 to 12 km. This depth range defines the seismogenic brittle zone of the crust. In section A1–A2 (Fig. 3b) a 40–50° angle, north-dipping cluster can be identified (shown by a red arrow), which was activated after 22 January 2010 (see Fig. 3a for a comparison). In sections B1–B2 and C1–C2, the clusters develop around the main shock hypocenters and form near-vertical structures. In section B1–B2, we note the existence of a high-angle cluster at depths between 10 and 17 km, with a 50–55° dip angle, The activated fault plane dips to the north and its surface projection lies to the south of the coastal Psathopyrgos fault (also north dipping; Doutsos and Poulimenos 1992; Houghton et al. 2003; Tsimi et al. 2007). This cluster was activated after 22 January 2010, as well. The along-strike seismicity profile defines an overall "trapezoidal" shape with is longest dimension at depth and extending 17 km in the along strike (ESE–WNW) direction. Figure 3c presents a larger-scale overview of the aftershock distribution (period 22 January–30 June 2010), where while reproducing the Fig. 3b features, it shows in better detail: (a) a south-dip imaged fault in the vicinity of the 22 January 2010 hypocenter (Fig. 3c, section C1–C2) in the depth range of 3–6 km; (b) moderate to high-angle, north-dipping faults in the range of depths of 7–12 km; (c) end of seismicity at depths larger than 12 km.

2.2 Geodetic data

We analyzed daily observations of the permanent GPS station EYPA near Efpalion, operated by Institut National des Sciences de l'Univers for the period 1 December 2009–1 March 2010 (Fig. 4). Code and phase data were processed with GAMIT/GLOBK software package (Herring et al. 2006). We included in our analysis data from 18 additional IGS stations (BRUS, CAGL, GRAZ, HERS, KIT3, MAS1, METS, PDEL, POL2, POTS, RABT, TRO1, WTZR, ZIMM, NICO, BUCU, ISTA, TELA) in order to serve as ties with the International Terrestrial Reference Frame 2005 (ITRF05; Altamimi et al. 2007). GAMIT uses double-differenced phase measurements (ionosphere-free linear combinations of the L1 and L2) to generate weighted least squares solutions for each daily session. Estimated

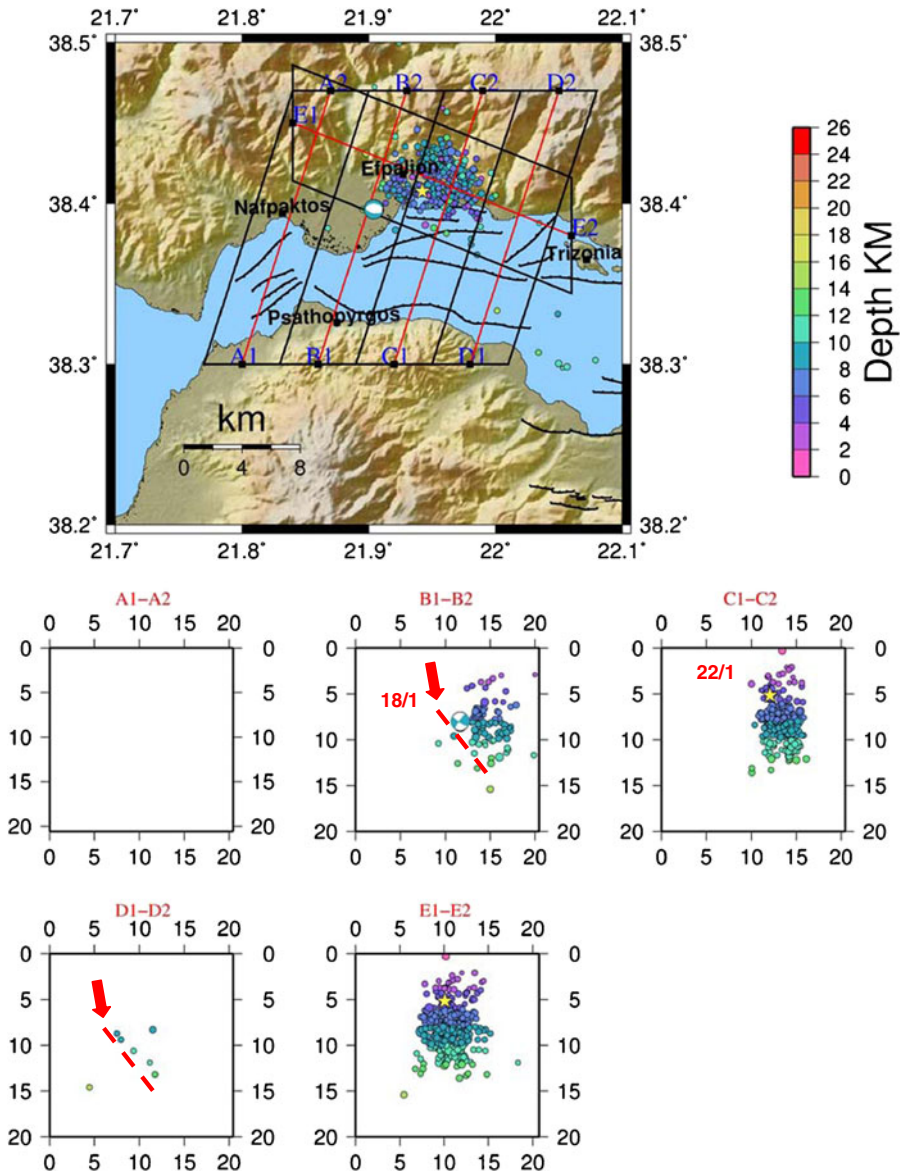

Fig. 3 **a** *Top* Map of the western Gulf of Corinth showing relocated epicenters of the Efpalio earthquake sequence (18–22 January 2010 period). Focal mechanism of the 18 January 2010 event is after Sokos et al. (2011). *Yellow stars* indicate mainshock epicenter of the second event. *Bottom* Graphs showing north–south cross-sections (*A1–A2*, *B1–B2*, *C1–C2*, and *D1–D2*) and ESE–WNW cross-section (*E1–E2*), respectively. Units in kilometer. **b** *Top* Map of the western Gulf of Corinth showing relocated epicenters of the Efpalio earthquake sequence (22 January–30 June2010, period). *Yellow stars* indicate main shock epicenters. *Bottom* Graphs showing *north–south* cross-sections (*A1–A2*, *B1–B2*, *C1–C2*, and *D1–D2*) and ESE–WNW cross-section (*E1–E2*), respectively. *Dotted red lines* in section *A1–A2* and *B1–B2* indicate seismic faults. *Red arrows* indicate north dip. Units in kilometer. **c** *Top* Enlargement and zoom towards the center of Fig. 3b showing relocated epicenters of the Efpalio earthquake sequence (22 January–30 June2010 period). *Yellow stars* indicate main shock epicenters. *Red triangle* indicates location of GPS station EYPA. *Bottom* Graphs showing north–south cross-sections. *Dotted red lines* in section *A1–A2*, *C1–C2*, and *F1–F2* indicate seismic faults. *Red arrows* indicate north-dipping faults. Units in kilometer

parameters include station coordinates, the six orbital elements for each satellite, Earth orientation parameters, and integer phase ambiguities. An automatic cleaning algorithm was applied to post-fit residuals in order to repair cycle slips and to remove outliers. The observation weights vary with elevation angle and are derived

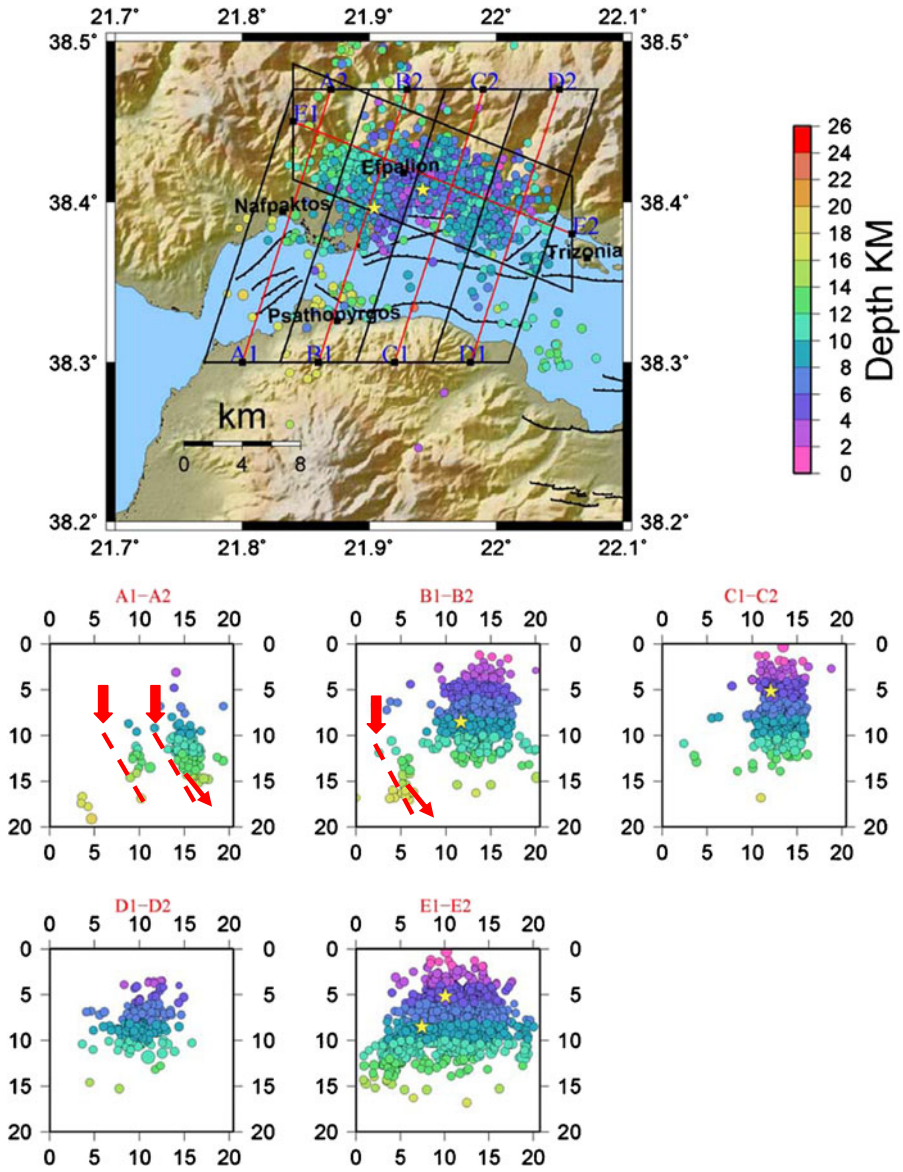

Fig. 3 (continued)

individually for each site from the scatter of post-fit residuals obtained in a preliminary GAMIT solution. We used a 10° elevation cutoff angle and atmospheric zenith wet delays were estimated every 2 h. We used the IGS absolute antenna phase center table for modeling the effective phase center of the receiver and satellites antennas and we applied the FES2004 ocean tide-loading model. The atmospheric propagation delay was modeled by means of Vienna mapping functions 1 (Boehm et al. 2006), and solid earth and polar tide corrections following the IERS/IGS standard 2003 model (McCarthy and Petit 2004). We used orbits provided (as g-files) by the Scripps Orbit Permanent Array Center (SOPAC). Next, the loosely constrained estimates and their covariances from each day were used as quasi-observations in GLOBK Kalman filter and combined with global and regional IGS and EUREF loosely constrained solutions provided by SOPAC. The reference frame was defined in the final step, applying generalized constraints while estimating a six-parameter transformation (six components of the rate of change of translation and rotation) by minimizing the departure of the horizontal velocities of the previously mentioned IGS sites from their a priori

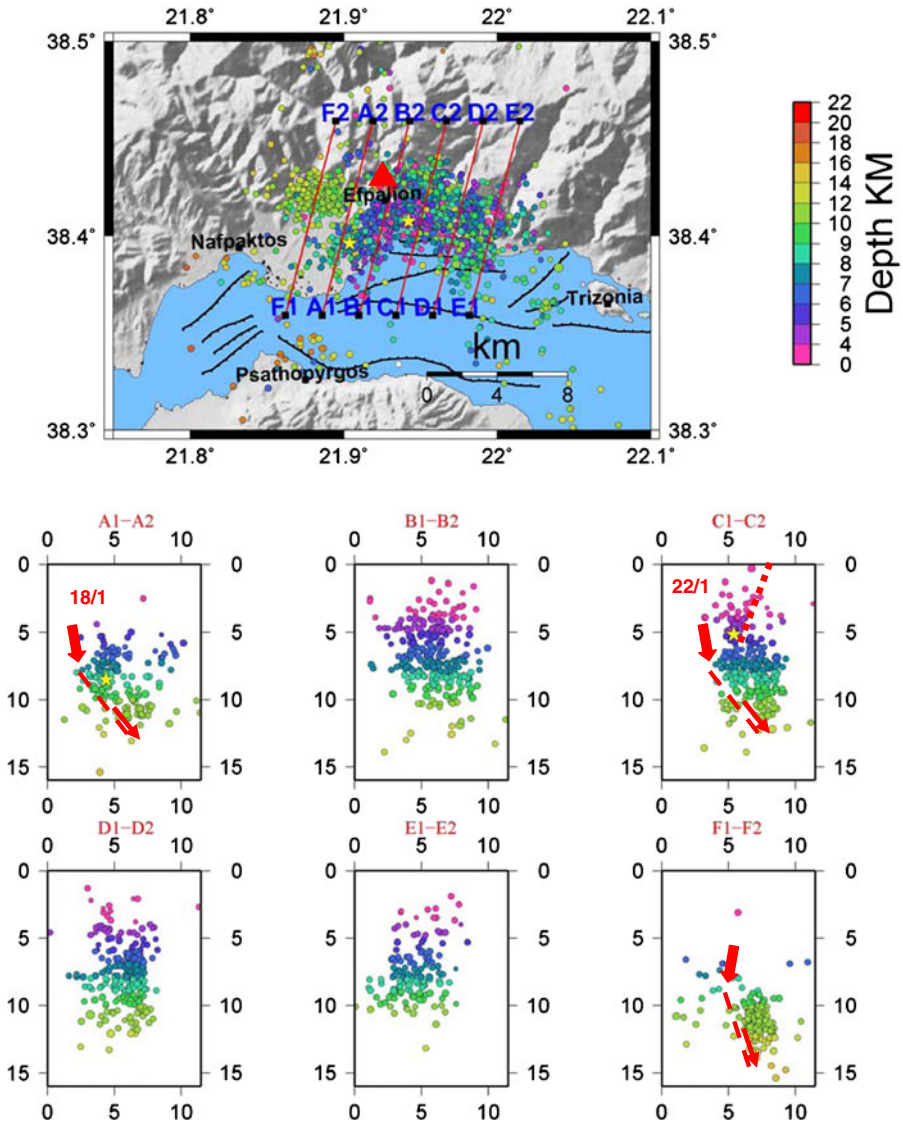

Fig. 3 (continued)

values given in the International Terrestrial Reference Frame 2005 (ITRF05). The final product of the analysis is three-component time series of daily station positions with respect to ITRF05.

The daily solutions of the static processing for the days before and after of the two events are reported in Table 3 (also in Fig. 4 in graphic form). Two coseismic offsets were detected corresponding to the 18–22 January 2010 earthquakes. To estimate the static coseismic displacements separately for the two events, we calculated the difference between the average position of 7 days before and 3 days after the earthquake of 18 January and the difference between the average position of 3 days before and 7 days after the event of 22 January. The displacements that occurred during the first event were 0.46 cm to the south, 0.51 cm to the east, and 1.73 cm downwards; while during the second event were 0.15 cm to the north, 0.35 cm to the east, and 1.84 cm downwards. These coseismic offsets are of the same order of magnitude, except for the north–south component where the second event caused very small displacement to the north, in contrast to the offset of the first event. We estimated the

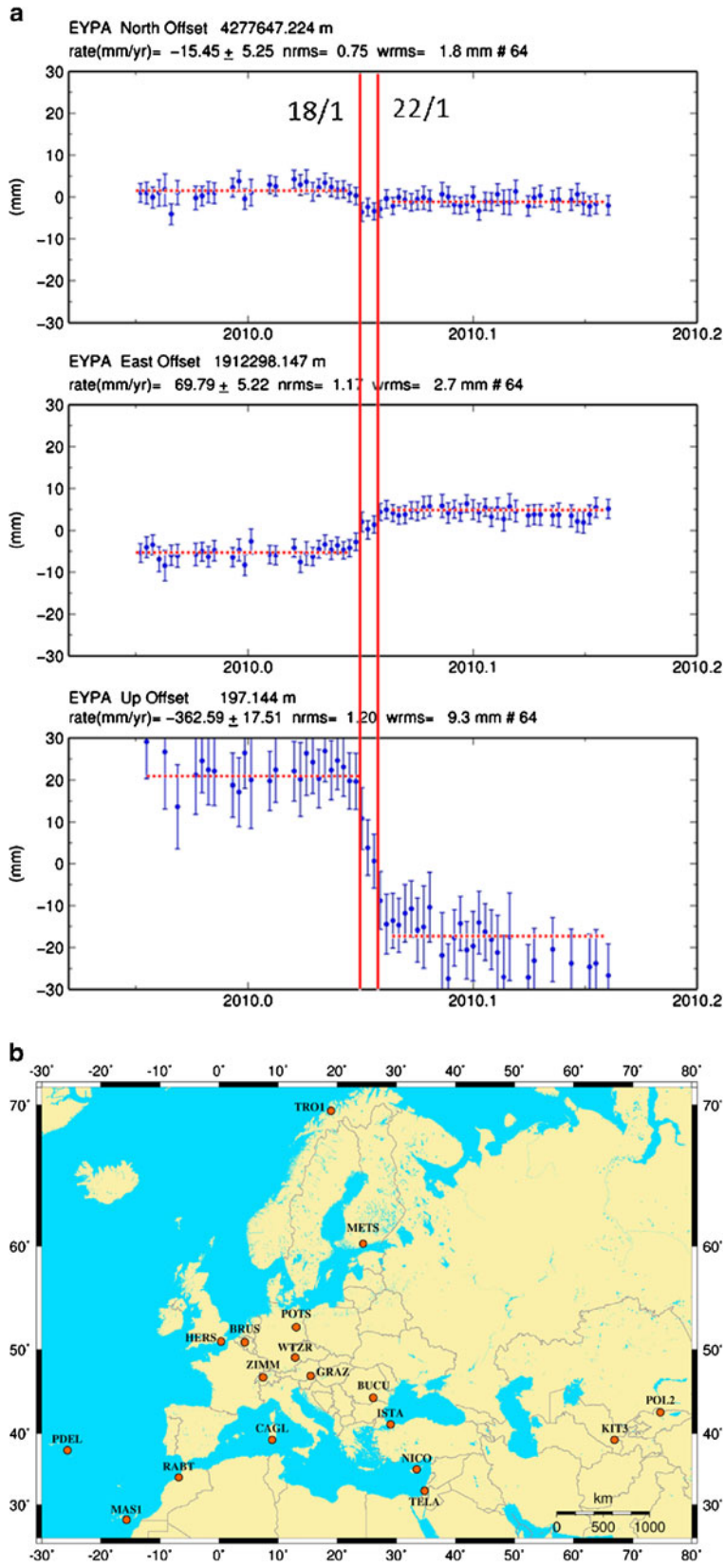

Fig. 4 **a** Displacement time series of INSU station EYPA (Efpalio). Each daily position is represented by a *blue dot* together with its $1-\sigma$ variation. *Red lines* indicate time of strong events. All three time-series are displaced across the red lines, which is interpreted as due to coseismic displacement (static). *Dotted red lines* indicate average position across the 18 and 22 January earthquakes. **b** Map showing distribution of IGS stations, used in GPS data processing

Table 3 Comparison of modeled coseismic surface displacements at the Efpalion GPS site versus the actual (observed) 30-s GPS measurements (Fig. 4)

	GPS difference D (17–22)	Model north/south (17–22)	Model south/south (17–22)	Model south/north 17–22
$u1$	−0.0030	−0.0024	−0.0025	−0.0020
$u2$	0.0086	0.0009	0.0009	0.0005
$u3$	−0.0362	−0.0071	−0.0073	−0.0067

Numbers 17–22 in the second row indicate the cumulative difference in GPS position from days 17 to 22 January 2010. The vector components are as follows: $u1$ is north–south (positive to north), $u2$ is east–west (positive to east) and $u3$ is up–down (positive upwards). North-dip plane characteristics are 270°/36°/−100°. South-dip plane is 102°/55°/−103°. For clarity, only the decimal part of the n, e, u local representation is shown. Units are in meters

total, average static displacement for both events, by fitting a line through the data points before and after the two mainshocks (Fig. 4, dotted red line). The total offset is 0.29 cm towards the south, 0.85 cm to the east, and 3.71 cm downwards (i.e., subsidence). $1-\sigma$ errors are 0.2 cm (north–south), 0.1 cm (east–west), and 0.5 cm (up–down), respectively. We note that the vertical displacement was accumulated through small offsets on 19, 20, and 21 of January 2010, respectively. Figure 5 shows the total motion of station EYPA from 17 to 22 January 2010. During the first event, the station moved to the SE. In the period between the two events, a small motion to the west is detected (about 1 mm). During the second event, the station moved to the NE with respect to its 18 January coseismic position. The overall motion was to the SE.

3 Coulomb stress modeling

Earthquakes have been observed to trigger subsequent earthquakes at short distances from the hypocenter by transferring static or dynamic stresses (e.g., Harris et al. 1995; Gomberg et al. 2001; Freed 2005; Parsons et al. 2006). We model stress transfer assuming that failure of the crust occurs by shear so that the mechanics of the process can be approximated by the Okada (1992) expressions for the displacement and strain fields due to a finite rectangular source in an elastic, homogeneous, and isotropic half space. In this paper, we compute the Coulomb stress change by assuming a shear modulus of 3×10^{10}Pa, Poisson's ratio 0.25, and two effective coefficients of friction ($\mu'=0.4$ and $\mu'=0.1$). We studied two cases of effective coefficient

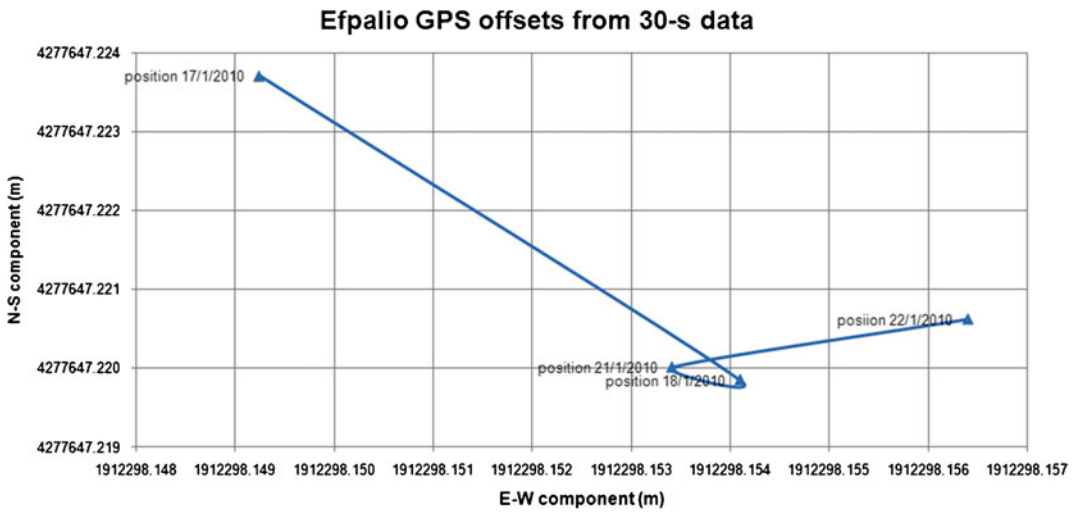

Fig. 5 Graph showing total motion of INSU station EYPA (Efpalio) on the horizontal plane during the earthquakes of 18 January and 22 January 2010. The measurements are reported in Table 7. Units are meter in local representation (n, e, u)

Table 4 Input parameters used for stress transfer modeling of the 18 January 2010 earthquake (M=5.1)

Poisson ratio	0.25
Shear modulus	G=30 GPa
Map projection	UTM zone 34
Depth of ΔCFF calculation	5 km (target is 22 January 2010 hypocenter) plane
Grid size	0.5 km
Friction coefficient (μ')	0.4 and 0.1
Horizontal length of rupture	3 km
Down–dip length of rupture	3 km
Azimuth of extension	187°
Regional stress	20 MPa [200 bar] (extensional)

of friction: μ'=0.4, which is closer to friction values for major faults (Harris and Simpson 1998) and μ'=0.1, which is closer to friction values on faults developed in weaker rheology. Details of the methodology can be found in previous works such as Ganas et al. (2008, 2010).

We calculated the change in the Coulomb failure function (CFF or Coulomb stress), on target failure planes (Reasenberg and Simpson 1992),

$$\Delta CFF = \Delta\tau + \mu'\Delta\sigma_\eta \quad (1)$$

where $\Delta\tau$ is the coseismic change in shear stress on the receiver fault and in the direction of fault slip, $\Delta\sigma_\eta$ is the change in the normal stress (with tension positive) and μ' is the effective coefficient of friction,

$$\mu' = \mu\left(1 - \Delta P/\Delta\sigma_\eta\right) \quad (2)$$

where μ is the coefficient of static friction and ΔP is the pore pressure change within the fault. From (2) it follows that, if ΔP=0 then μ'=μ. ΔCFF is the Coulomb stress change between the initial (ambient) stress and the final stress. If the dislocation model (Table 4) is thought of as an earthquake rupture, the ambient field is the field that existed before the earthquake and the total field is the sum of the ambient field plus the earthquake-induced stresses.

3.1 Triggering of the 22 January 2010 earthquake

We computed Coulomb stress change caused by the 18 January 2010 event on optimally oriented planes to regional extension. A value of 20 MPa was adopted as regional stress magnitude to provide a stress level well above the average static stress drop of moderate–large earthquakes (3–4 MPa; Kanamori and Anderson 1975; Allman and Shearer 2009). For extension azimuth, we adopted the orientation of the T axis of the focal plane solution of the 18 January 2010 event (N187° E; Table 4). The calculation was done at seismogenic depths (5–11 km range) including the depth of the 22 January 2010 event hypocenter (5 km). The target planes are similar in orientation to the 18 January 2010 fault plane, i.e., they strike east–west and dip either to the north or to the south. Next, we run *elfgrid* to calculate the stress tensor on horizontal observation planes. The output is six grids, one for each component of the tensor. Then, we calculate the change in the CFF on optimal failure planes at 5–11 km range of depths by running *stroop* (stress_on_optimal_planes). ΔCFF was sampled on a 20×20 km grid, with 0.5 km grid spacing. A uniform slip model provided by Sokos et al. (2011, 2012) was used. As a slip surface, we assumed a square, planar source with dimensions 3×3 km and a

Table 5 Parameters of statistical analysis of ΔCFF at depth 5 km, hypocenter area of 22 January 2010 event (40,400 grid points) after applying stress on optimal planes method

Parameter	μ'=0.1	μ'=0.4
Mean value of ΔCFF	2.8 KPa (0.028 bar)	2.5 KPa (0.025 bar)
Standard deviation	9.8 KPa (0.098 bar)	10.7 KPa (0.107 bar)
Minimum of ΔCFF	−11.9 KPa (−0.119 bar)	−17.5 KPa (−0.175 bar)
Maximum of ΔCFF	81.9 KPa (0.817 bar)	101.9 KPa (1.019 bar)
Range of ΔCFF	93.6 KPa (0.936 bar)	119.5 KPa (1.195 bar)
ΔCFF at 22 January 2010 hypocenter (optimal planes)	32.9 KPa (0.329 bar)	34.1 KPa (0.341 bar)
ΔCFF at 22 January 2010 hypocenter (reactivated planes)	22 KPa (0.220 bar)	31 KPa (0.310 bar)

We can see that by increasing the coefficient of friction, ΔCFF is increased. For methods, see Ganas et al. (2010)

uniform slip of 0.21 m. This set of parameters provides a seismic moment of 5.67×10^{23} dyncm which is very close to the moments calculated by both NOA (5.59×10^{23} dyncm) and AUTH (8.49×10^{23} dyncm). The catalog of the aftershocks used for investigating seismicity triggering was produced by relocation of HUSN events (Fig. 3).

For the 18 January 2010 earthquake, we estimated an average, right-lateral strike-slip displacement (u_s) of 0.036 m and a dip-slip displacement (u_d) of 0.206 m for a magnitude M_w = 5.1-5.2, by using the Hanks and Kanamori formula (1979):

$$M_w = (2/3) \times (\log Mo - 16.05) \quad (3)$$

where M_o is the scalar moment of the best double couple in dyne centimeter. Seismic moment is given by the following equation:

$$Mo = G \times A \times u \quad (4)$$

where A is fault area, G is shear modulus and u is total displacement. We assumed an asperity of 9 km^2 (3×3 km wide rupture) which is close to what was suggested by Sokos et al. (2011), who used a slip inversion method. The two components of displacement vector are calculated from the following formulas given the slip models in Table 6:

$$u_s = \cos(rake) \times u \quad (5)$$

$$u_d = -\sin(rake) \times u \quad (6)$$

The parameters considered for the stress change computation are given in Table 5, while the stress change maps are presented in Fig. 6.

Fig. 6 Maps of Coulomb Stress following the 18 January 2010 Efpalio earthquake (M_w=5.1) at various depths inside the upper crust (from top to bottom the maps are at depths of 5, 6, 7, 8 9, 10, and 11 km). *Reddish* colors indicate loading, *bluish* colors indicate unloading, respectively. **a** The model assumes a coefficient of friction of 0.1 along the fault plane; **b** the model assumes a friction of 0.4. Coulomb stress has been calculated for optimal planes to regional extension (N187° E). **c** Map of Coulomb stress transfer for reactivated planes with the 22 January 2010 slip model. *Green circles* represent aftershock hypocenters for the period 18–22 January 2010 and at the depth of the map ±500 m to account for hypocentral error. It is clearly seen that the majority of aftershocks occurred on loaded areas of the crust. Aftershocks were relocated using HypoDD software. *Vertical yellow line* indicates cross-section shown in Fig. 7a. *Vertical red line* indicates cross-section shown in Fig. 7b; 1 bar=100 kPa

The stress change was computed for two cases for the coefficient of apparent friction: 0.1 (Fig. 6a, top) and 0.4 (Fig. 6b, bottom) to account for possible differences on the material properties along the fault planes. We found no significant difference on stress patterns; however, the actual stress values are larger for friction=0.4. In both cases, Coulomb stress increases laterally (i.e., along the 18 January 2010 rupture) and decreases orthogonally (i.e., across the rupture). At 7–10 km depth, Coulomb stress load exceeds 350 KPa near rupture tips. Most (over 80 %) relocated aftershocks in the depth range of 5–10 km are located inside loaded areas. We also constructed cross-sections of Coulomb stress-oriented north–south to get a 3-D view of the stress field normal to the 18 January 2010 rupture (Fig. 7). The cross-sections show loading of the crust above and below the rupture. We observe that many, off-fault 18–22 January relocated aftershocks occurred inside loaded areas of the upper crust and to the down-dip direction (Fig. 7 top). The aftershocks are occupying mostly a vertical volume of material and occur at distances as

Table 6 Efpalio earthquake focal parameters published by various organizations – institutes on the Internet

Date	Depth (km)	M_w	Scalar moment	Strike/dip/rake Plane 1	Strike/dip/rake Plane 2	Source
18/1/2010	6.6	5.3		102°/55°/−83°	270°/36°/−100°	Sokos et al. (2011)
	13.5	5.5	1.98E+24	94/45/−95	282/45/−85	INGV
	12.2	5.5	2.00E+24	301/49/−49	68/55/−127	HARV
	4	5.2	8.49E+23	271/48/−100	107/43/−79	AUTH
	5	5.1	5.59E+23	103/40/−73	261/52/256	NOA
	16	5.3	9.93E+23	254/28/−123	111/67/−74	UPSL
22/1/2010	8	5.2		78°/40°/108°	282°/52°/−75°	Sokos et al. (2011)

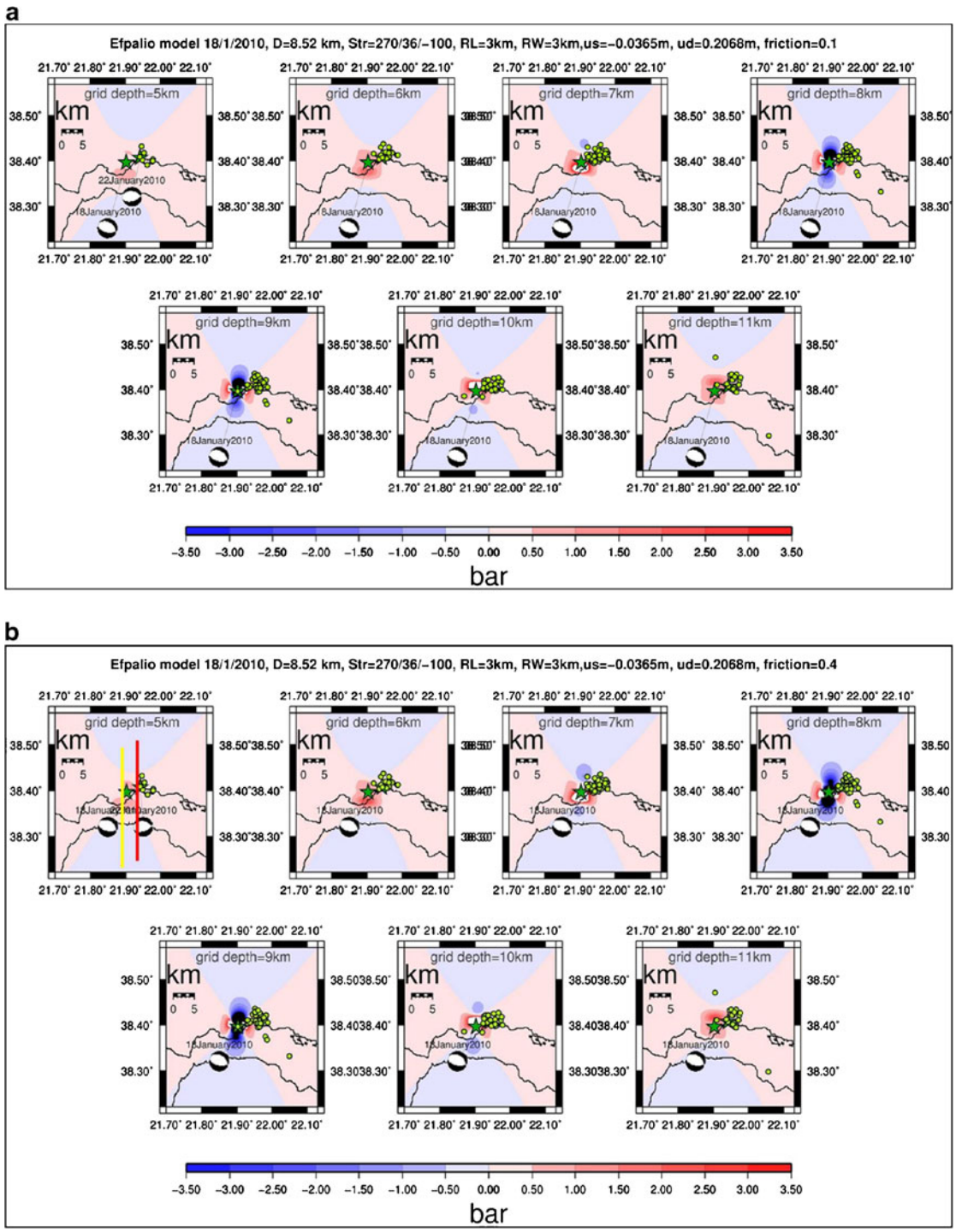

much as 6–8 km from the 18 January hypocenter (Fig. 7). Aftershocks occurring inside the relaxed area (both north and south of the seismic fault; right and left from the fault plane depicted in Fig. 7 top) are not explained by our slip model but could be due to (a) missed heterogeneous slip that modifies the static stress transfer change across the fault, (b) on damage in the vicinity of the rupture (brittle microcracking), (c) dynamic stress triggering (Gomberg et al. 2001), or the location uncertainty of the catalog (Catalli and Chan

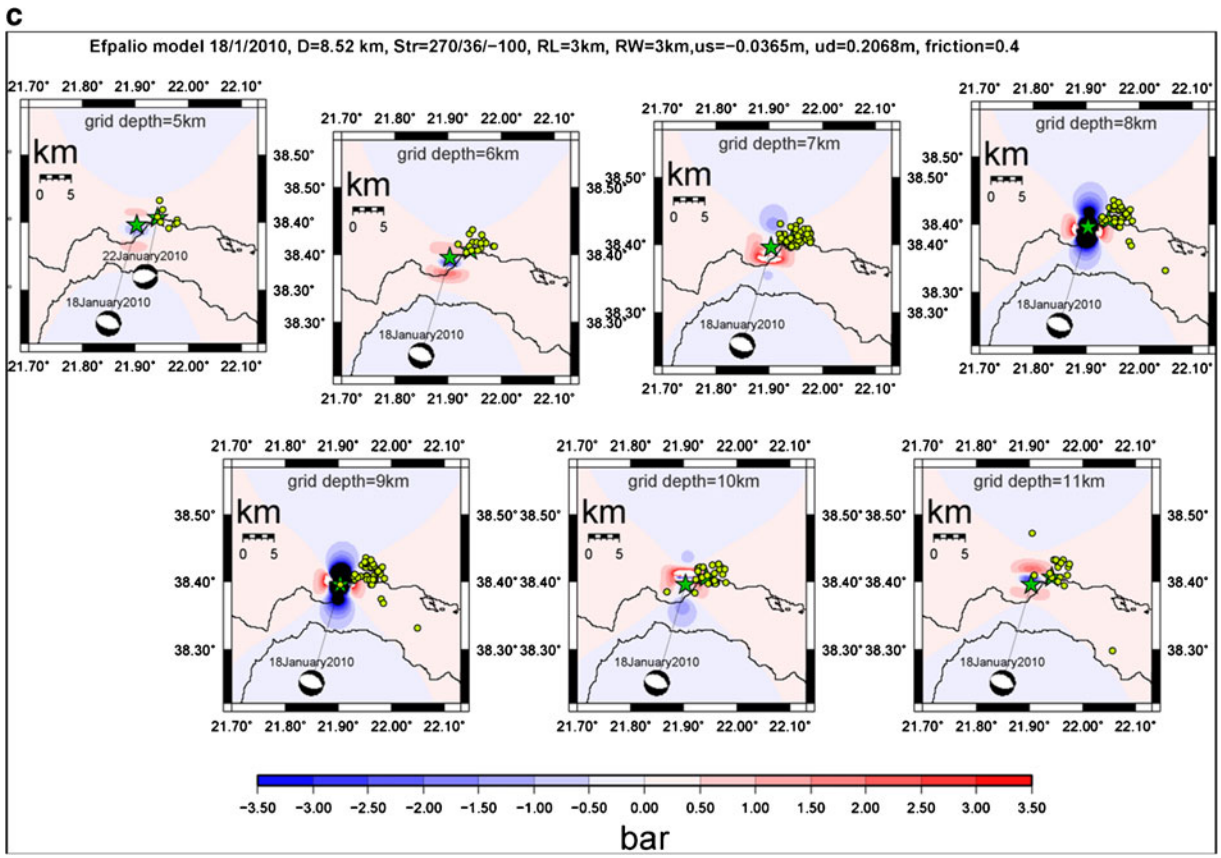

Fig. 6 (continued)

2012). The stress section going through the 22 January 2010 (Fig. 7b) shows that this area received a Coulomb stress of circa 34 KPa so it was brought closer to failure. We interpret the occurrence of the 22 January 2010 main shock as a result of static triggering by the 18 January 2010 event.

As a variation, Coulomb stress can be calculated on planes of fixed orientation if it is known that there is a fabric of existing normal faults in the western Gulf of Corinth area which are likely to provide planes of failure. In this case, we assume that east–west striking, south-dipping normal faults of the 22 January 2010 type of rupture will be of interest as candidates for failure. We use *strop* (stress_on_planes) in this run to calculate Coulomb stress on planes of specified orientation at 5–11 km depth (Fig. 6c). We found that triggering is also promoted as the ΔCFF values were positive in the hypocentral area of the 22 January 2010 earthquake (between 22 and 31 KPa; see Table 5). This result further supports our proposal that the 22 January 2010 earthquake in Efpalio was promoted by the 18 January 2010 event.

4 Discussion

4.1 Seismic fault modeling

The geodetic results were examined for identifying the source of deformation. For the 18 January 2010 event, the results of the GPS processing showed a coseismic displacement of 0.45 cm towards the south, 0.51 cm towards the east, and 1.73 cm subsidence (Table 7). The offsets for the 22 January 2010 event are 0.14,

Fig. 7 Cross-sections of Coulomb stress following the 18 January 2010 Efpalio earthquake (M_w=5.1) in the north–south direction passing through the 18 January epicenter (*top*; **a**) and 22 January epicenter (*bottom*; **b**); 1 bar=100 KPa. *Reddish colors* indicate loading, *bluish colors* indicate unloading, respectively. Unit axes are in kilometer. We assume a friction of 0.4. Coulomb stress has been calculated for optimal planes to regional extension (N187° E). *Brown circles* represent aftershock hypocenters for the period 18–22 January 2010. *Green stars* are main shock hypocenters. It is clearly seen that the majority of aftershocks occurred on loaded areas of the crust. A value of 0.34 bar [34 KPa] is obtained for the hypocentral area of the 22 January 2010 event

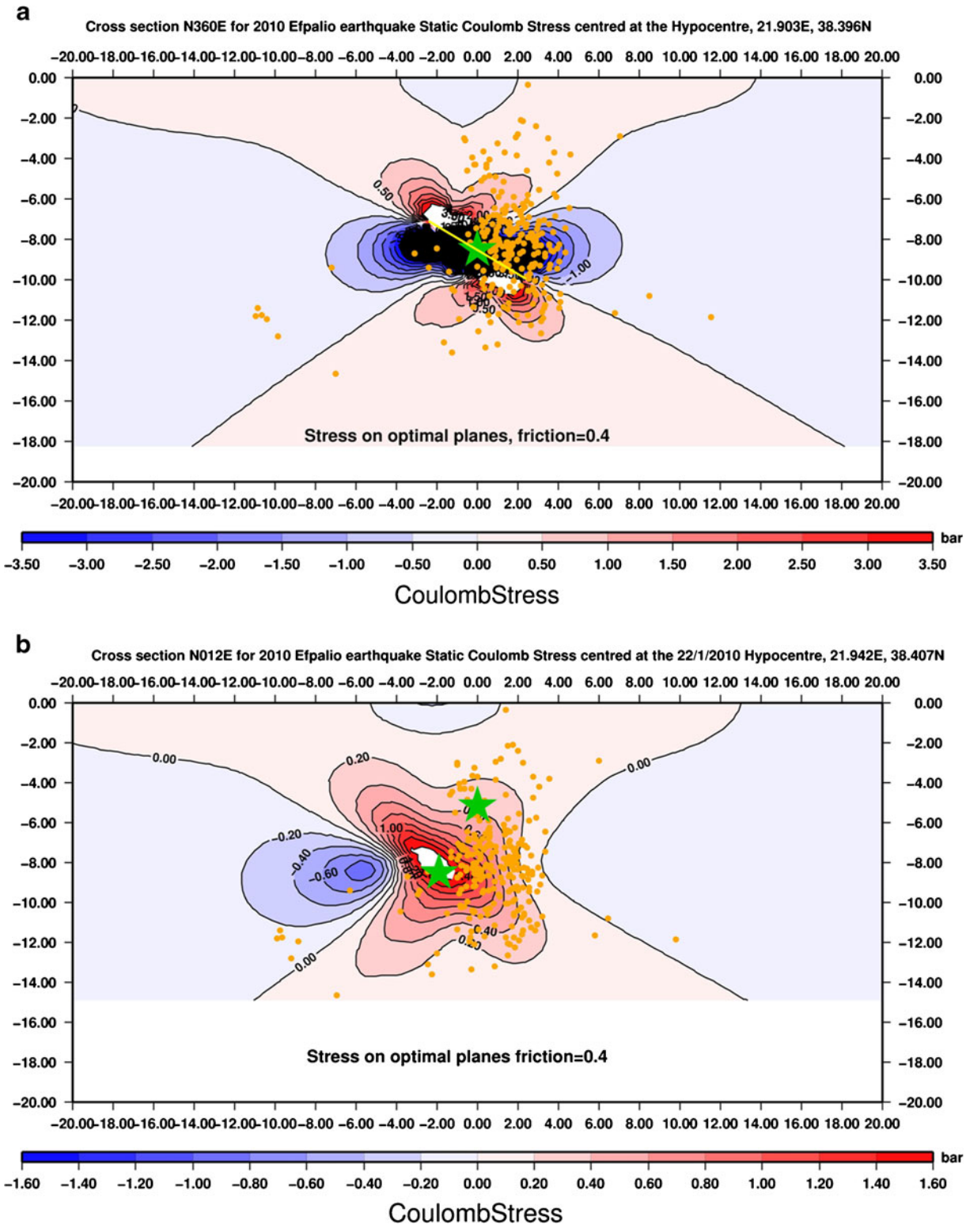
a
Cross section N360E for 2010 Efpalio earthquake Static Coulomb Stress centred at the Hypocentre, 21.903E, 38.396N
Stress on optimal planes, friction=0.4
bar
CoulombStress
b
Cross section N012E for 2010 Efpalio earthquake Static Coulomb Stress centred at the 22/1/2010 Hypocentre, 21.942E, 38.407N
Stress on optimal planes friction=0.4
bar
CoulombStress

Table 7 Coseismic offsets of Efpalion GPS station

	Day before	Day after	Day before	Day after	Difference	Difference	Total difference
	17	18	21	22	D (17–18)	D (21–22)	D (17–22)
$u1$	4,277,647.22506	4,277,647.22055	4,277,647.22055	4,277,647.22202	0.00451	−0.00147	−0.00304
$u2$	1,912,298.14798	1,912,298.15311	1,912,298.15311	1,912,298.15659	−0.00513	−0.00348	0.00861
$u3$	197.13052	197.11327	197.11327	197.09432	−0.01725	−0.01895	−0.0362

Displacement components are given in local representation (n, e, up). The following convention is used: $u1$ is north–south component, $u2$ is east–west, and $u3$ is up–down. Units are in meters

0.34, and 1.89 cm, respectively. We compare these results with forward models for surface deformation in an elastic half-space based on Okada (1992) and using as inputs the focal plane solutions for both events provided by Sokos et al. (2012). Due to the 500-m grid size of our elastic model, we could compare a point located about 300 m from the GPS site. Station GPS EYPA is located at 38.4268 N, 21.9281E while our forward model point is located at 38.4247169 N, 21.9262409E, i.e., ΔL=0.2826 km. We find that the worst performance is given by the combination of a south-dipping fault for the first event and a north-dipping fault for the second event (Table 3; this was suggested by Sokos et al. 2012). The other two models (a north-dipping fault for the first event and a south-dipping fault for the second event or a south-dipping fault for the first event and a south-dipping fault for the second event) perform almost equally with submillimeter differences. However, both these two slip models underestimate the surface displacements in components $u2$ (east–west) and $u3$ (vertical; Table 3). The east–west modeled components are a factor of 10 less than GPS values while the up–down component is less by a factor of 5. This discrepancy is due to either (a) the isotropic and elastic structure of the upper crust assumed in the forward model, (b) the uniform slip model used, or (c) a combination of both. So, in this respect, the GPS static displacements are inconclusive of the geometry of the 18–22 January 2010 fault planes.

However, our relocated seismicity data (Fig. 3) suggests that the first event ruptured a blind, north-dipping normal fault beneath the north shore of the Gulf, near Efpalio because of the preferential location of the aftershock hypocenters in the hangingwall area of the north-dipping imaged fault (see B1–B2 cross-section in Fig. 3a), irrespective of the velocity model used in relocation (i.e., Patras, Latorre et al. 2004; Rigo et al. 1996). The dip attribute is not well constrained by the relocation and it may attain a value between 36° and 48° (see Table 6 for a summary of focal plane solutions). A similar conclusion was reached by Karakostas et al. (2012). The second event (22 January 2010) occurred on a different normal fault, also blind, but not easy to image its geometry from our datasets. The only evidence available is the post-22 January 2010 aftershock pattern aligned along a south-dipping fault in section C1–C2 of Fig. 3c. Karakostas et al. (2012) suggest a north-dipping fault hosting the second event as well.

It is also interesting to point out the existence of north-dipping, high-angle faults at 10–15 km depths, which were reactivated because of Coulomb stress transfer, to the west and south of Efpalion (see A1–A2/B1–B2 cross-sections in Fig. 3b and section F1–F2 in Fig. 3c). This evidence may be considered in the investigations on the nature of extension in this area and on the importance of high-angle faulting in active deformation (e.g., Bell et al. 2009, 2011; Vassilakis et al. 2011; Taylor et al. 2011; Fig. 1).

4.2 Seismicity rate patterns in the western Gulf of Corinth

The occurrence of the 2010 events signifies the end of the seismic quiescence in this area of the Gulf of Corinth so we conducted a statistical analysis of the regional earthquake catalog to search for rate anomalies. For this task, we analyzed the NOA catalog data (spanning a period of 40 years) in order to investigate seismicity rate changes and associated stress levels (e.g., Wyss et al. 2008). The recently compiled earthquake catalog for the 37.00–39.00 N and 19.00–23.50 E regions from 1964 until 2008 (Chouliaras 2009b) was used. Here, we follow the same methodology as in Chouliaras (2009a, b), using the ZMAP software package (Wiemer 2001) and found that in this area of Greece and for depths of 0–50 km, our

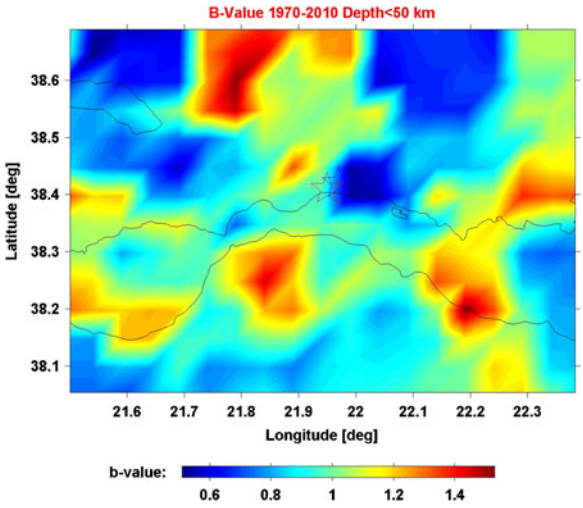

Fig. 8 The *b* value map for the investigated region based on the NOA-IG earthquake catalog starting at the value of 1,970.0. For plotting the *b* value map, we used a sample of $N=100$ events per node with grid spacing=0.05° (approximately 5 km per node). The *gray stars* indicate the epicenters of the 18 and 22 January 2010 main shocks, respectively

catalog has a magnitude of completeness of 3.0±0.1 (M_c; Wiemer and Wyss 2000). We also applied the declustering algorithm of Reasenberg (1985) to remove aftershocks and swarms.

Our analysis (Fig. 8) shows that the 2010 Efpalio earthquakes are located inside a relatively low *b* value area inside the western Gulf of Corinth (*b* ranges from 0.6 to 0.8 near Efpalion, while the value for the total NOA catalog is 1.14; Chouliaras 2009b). The *b* value is the slope of the linear fit to the frequency–magnitude distribution of earthquakes [$\log_{10}N=a-bM$; Gutenberg and Richter 1944]. It describes the relative size of the seismic events and in this paper it was determined by the maximum-likelihood technique following Aki (1965). The *b* value exhibits heterogeneities in time and space, depending on the stress patterns and in this way it acts as a stress meter (Schorlemmer et al. 2005) where low *b* values indicate high-stress regimes (Wyss et al. 2008). We find reasonable to associate the 15-year-old quiescence to the low *b* value of the Efpalion crust, although we cannot estimate its depth dependence. In the western Gulf of Corinth, a low *b* value was also found by Wyss et al. (2008) for depths greater than 8 km, using a local seismicity catalog.

4.3 Magnitude scaling properties of aftershocks

The energy properties of the aftershock sequence are also important. It is interesting to note that for the first 259 well-located events of the aftershock sequence (18–22 January 2010; Fig. 3a) no scaling is observed between earthquake (aftershock) size and distance to main shock, over 3 orders of magnitude (Fig. 9). Earthquake size ranges for $1.9<M<4.1$ and distance to main shock from $0.05<L<8.18$ km. We find no spatial decay of local earthquake magnitude over nearly 2.5 fault lengths with respect to the 18 January 2010 seismic fault (we used a homogeneous

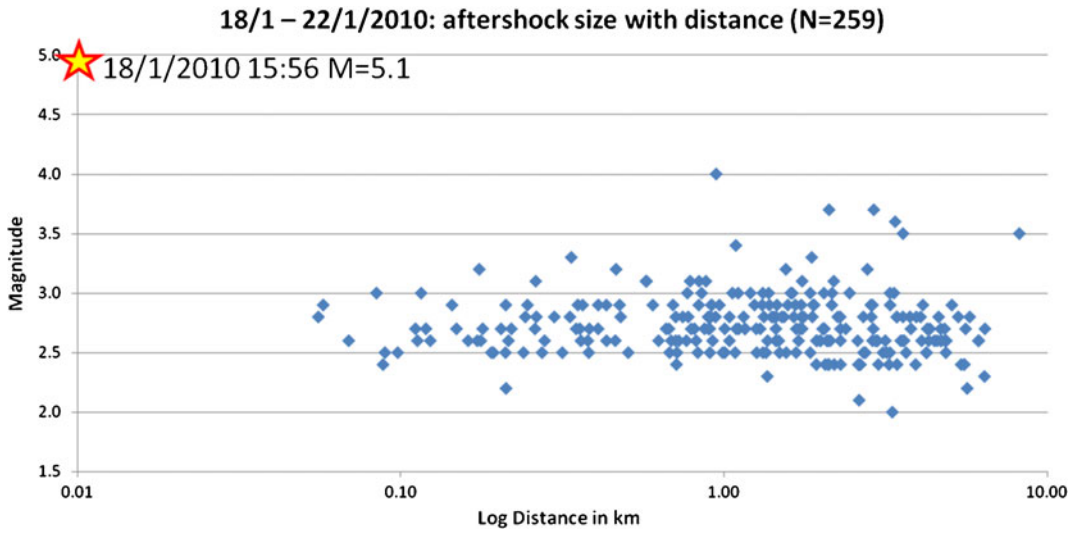

Fig. 9 Graph showing no decay of aftershock size with distance for the first 3.5 days of the Efpalio sequence. *X*-axis is distance to main shock. *Y*-axis is local magnitudes

slip model 3×3 km; Table 4). This observation may favor a dynamic stress transfer triggering mechanism (Felzer and Brodsky 2006) for most of the first 4-day aftershocks versus a static stress triggering scenario where a magnitude scaling with distance would fit the decay of radiated seismic strains, although a more detailed statistical analysis is necessary to clarify this point.

5 Conclusions

1. The 18 January 2010, 15:56 UTC M_w=5.1 (NOA) Efpalio event ruptured a blind normal fault which transferred 22–34 KPa Coulomb stress to trigger the 22 January 2010, 00:46 UTC M_w=5.1 (NOA) event, about 3 km to the NE.
2. The two M=5.1 events produced combined, permanent static displacement of station EYPA (Efpalio) of 0.3 cm towards the south, 0.8 cm to the east and 3.6 cm downwards (i.e., subsidence).
3. The early aftershock pattern (Fig. 3) favors an 18 January 2010 seismic fault dipping to the north. The post-22 January 2010 aftershock pattern is dispersed with limited evidence for a south-dipping fault at depths 3–7 km in the vicinity of the 22 January 2010 hypocenter.
4. We also point out the existence of north-dipping, high-angle faults at 10–15 km depths, which were reactivated because of Coulomb stress transfer, to the west and south of Efpalion.
5. The 2010 Efpalio events occurred in a low b value area (0.6–0.8) of the Gulf of Corinth that may be identified with a high concentration of crustal stress.
6. The 4-day aftershock sequence (period between 18 and 22 January 2010) shows no spatial decay of magnitude with distance from main shock, over 2.5 fault lengths.

Acknowledgments We thank E. Sokos for discussions and Institut National des Sciences de l'Univers/ENS for providing the 30-s rinex files for the Efpalio station. X. Ventouzi helped with HypoDD processing. We acknowledge Bob Simpson for making available the DLC code, Ioannis Kalogeras, Tom Herring and Tom Parsons for useful comments. We thank three anonymous reviewers and the Associate Editor for extensive reviews. The open-source software GMT http://www.soest.hawaii.edu/gmt/ was used to make figures. The GPS data were downloaded from https://gpscope.dt.insu.cnrs.fr/chantiers/corinthe/. We dedicate this paper to the memory of our student Yannis Adamis who passed away on April 5, 2010.

References

Aki K (1965) Maximum likelihood estimate of b in the formula log N=a - bM and its confidence limits. Bull Earthq Res Inst Univ Tokyo 43:237–239

Allman BP, Shearer PM (2009) Global variations of stress drop for moderate to large earthquakes. J Geophys Res 114: B01310

Altamimi Z, Collilieux X, Legrand J, Garayt B, Boucher C (2007) ITRF2005: a new release of the International Terrestrial Reference Frame based on time series of station positions and Earth orientation parameters. J Geophys Res 112:B09401

Avallone A, Briole P, Agatza-Balodimou AM, Billiris H, Charade O, Mitsakaki C, Nercessian A, Papazissi K, Paradissis D, Veis G (2004) Analysis of eleven years of deformation measured by GPS in the Corinth Rift Laboratory area, C.R. Geoscience 336:301–312

Baumont D, Scotti O, Courboulex F, Melis N (2004) Complex kinematic rupture of the M_w 5.9, 1999 Athens earthquake as revealed by the joint inversion of regional seismological and SAR data. Geophys J Int 158:1078–1087

Bell RE, McNeill L, Bull JM, Henstock TJ, Collier REL, Leeder MR (2009) Fault architecture, basin structure and tectonic evolution of the Corinth rift, central Greece. Basin Res 21:824–855

Bell RE, McNeill LC, Henstock TJ, Bull JM (2011) Comparing extension on multiple time and depth scales in the Corinth Rift, Central Greece. Geophys J Int 186:463–470

Bernard P, Briole P, Meyer B, Lyon-Caen H, Gomez J-M, Tiberi C, Berge C, Cattin R, Hatzfeld D, Lachet C, Lebrun B, Deschamps A, Courboulex F, Larroque C, Rigo A, Massonnet D, Papadimitriou P, Kassaras J, Diagourtas D, Makropoulos K, Veis G, Papazisi E, Mitsakaki C, Karakostas V, Papadimitriou E, Papanastassiou D, Chouliaras G, Stavrakakis G (1997) The M_S=6.2, June 15, 1995 Aigion earthquake (Greece): evidence for law angle normal faulting in the Corinth rift. J Seismol 1:131–150

Boehm J, Werl B, Schuh H (2006) Troposphere mapping functions for GPS and very long baseline interferometry from European Center for Medium-Range Weather Forecasts operational analysis data. J Geophys Res 111:B02406

Briole P, Rigo A, Lyon-Caen H, Ruegg JC, Papazissi K, Mitsakaki C, Balodimou A, Veis G, Hatzfeld D, Deschamps A (2000) Active deformation of the Corinth Rift, Greece: results from repeated global positioning system surveys between 1990 and 1995. J Geophys Res 105:605–625

Catalli F, Chan CH (2012) New insights into the application of the Coulomb model in real-time. Geo J Int 188. doi:10.1111/j.1365-246X.2011.05276.x

Chiarabba C, Amato A, Anselmi M, Baccheschi P, Bianchi I, Cattaneo M, Cecere G, Chiaraluce L, Ciaccio MG, De Gori P, De Luca G, Di Bona M, Di Stefano R, Faenza L, Govoni A, Improta L, Lucente FP, Marchetti A, Margheriti L, Mele F, Michelini A, Monachesi G, Moretti M, Pastori M, Piana Agostinetti N, Piccinini D, Roselli P, Seccia D, Valoroso L (2009) The 2009 L'Aquila (central Italy) MW 6.3 earthquake: main shock and aftershocks. Geophys Res Lett 36: L18308

Chouliaras G (2009a) Seismicity anomalies prior to the 13 December 2008, M_S=5.7 earthquake in Central Greece. Nat Hazards Earth Syst Sci 9(2):501–506

Chouliaras G (2009b) Investigating the earthquake catalog of the National Observatory of Athens. Nat Hazards Earth Syst Sci 9:905–912

Doutsos T, Poulimenos G (1992) Geometry and kinematics of active faults and their Seismotectonic significance in the western Corinth-Patras rift (Greece). J Struct Geol 14 (6):689–699

Doutsos T, Koukouvelas IK, Xypolias P (2006) A new orogenic model for the external Hellenides, in Tectonic Development of the Eastern Mediterranean Region. In: Robertson AHF (ed) Demosthenis Mountrakis, Geological Society. Special Publication, London, pp 507–520, 260

Felzer KR, Brodsky EE (2006) Decay of aftershock density with distance indicates triggering by dynamic stress. Nature 441:735–738. doi:10.1038/nature04799

Freed AM (2005) Earthquake triggering by static, dynamic, and postseismic stress transfer. Annu Rev Earth Planet Sci 33-335

Ganas A, Gosar A, Drakatos G (2008) Static stress changes due to the 1998 and 2004 Krn Mountain (Slovenia) earthquakes and implications for future seismicity. Nat Hazards Earth Syst Sci 8:59–66

Ganas A, Serpelloni E, Drakatos G, Kolligri M, Adamis I, Tsimi C, Batsi E (2009) The M_w 6.4 SWAchaia (Western Greece) Earthquake of 8 June 2008: Seismological, Field, GPS Observations, and Stress Modeling. J Earthq Eng 13(8):1101–1124

Ganas A, Grecu B, Batsi E, Radulian M (2010) Vrancea slab earthquakes triggered by static stress transfer. Nat Hazards Earth Syst Sci 10:2565–2577

Gallovič F, Zahradník J, Křížová D, Plicka V, Sokos E, Serpetsidaki A, Tselentis G-A (2009) From earthquake centroid to spatial-temporal rupture evolution: M_w 6.3 Movri Mountain earthquake, June 8, 2008, Greece. Geophys Res Lett 36:L21310

Gomberg J, Reasenberg PA, Bodin P, Harris RA (2001) Earthquake triggering by seismic waves following the Landers and Hector mine earthquakes. Nature 411:462–466

Gutenberg B, Richter CF (1944) Frequency of earthquakes in California. Bull Seismol Soc Am 34:185–188

Hanks TC, Kanamori H (1979) A moment magnitude scale. J Geophys Res 84:2348–2350

Harris RA, Simpson RW (1998) Suppression of large earthquakes by stress shadows: a comparison of coulomb and rate-and-state failure. J Geophys Res 103:24439–24451

Harris RA, Simpson RW, Reasenberg PA (1995) Influence of static stress changes on earthquake locations in southern California. Nature 375:221–224

Hatzfeld D, Kementzetzidou D, Karakostas V, Ziazia M, Nothard S, Diagourtas D, Deschamps A, Karakaisis G, Papadimitriou P, Scordilis M, Smith R, Voulgaris N, Kiratzi S, Makropoulos K, Bouin M-P, Bernard P (1996) The Galaxidi earthquake of 18 November, 1992: a possible asperity within the normal fault system of the Gulf of Corinth (Greece). Bull Seismol Soc Am 86:1987–1991

Herring TA, King RW, McClusky SC (2006) Introduction to GAMIT/GLOBK, Release 10.3, Department of Earth Atmosphere and Planetary Sciences, Massachusetts Institute of Technology, Cambridge, Mass

Houghton SL, Roberts GP, Papanikolaou ID et al (2003) New U-234-Th-230 coral dates from the western Gulf of Corinth: implications for extensional tectonics. Geophys Res Lett 30. doi:10.1029/2003GL018112

Jansky J, Zahradnik J, Sokos E, Serpetsidaki A, Tselentis GA (2004) Relocation of the 2001 earthquake sequence in Aegion, Greece. Stu Geophys Geod 48:331–344

Kanamori H, Anderson DL (1975) Amplitude of the Earth's free oscillations and log-period characteristics of earthquake source. J Geophys Res 80(8):1075–1078

Karakostas V, Karagianni E, Paradisopoulou P (2012) Space–time analysis, faulting and triggering of the 2010 earthquake doublet in western Corinth Gulf. Nat Hazard 63:1181–1202

Kiratzi A, Sokos E, Ganas A, Tselentis A, Benetatos C, Roumelioti Z, Serpetsidaki A, Andriopoulos G, Galanis O, Petrou P (2008) The April 2007 earthquake swarm near Lake Trichonis and implications for active tectonics in western Greece. Tectonophysics 452:51–65

Klein FW (2002) User's Guide to HYPOINVERSE–2000, a Fortran Program to Solve for Earthquake Locations and Magnitudes, U.S. Geological Survey, Open-File Report 02–171

Koukouvelas I, Kokkalas S, Xypolias P (2009) Surface deformation during the M_w 6.4 (June 08, 2008) Movri Mt earthquake, Greece. Int Geol Rev 52:249–268

Latorre D, Virieux J, Monfret T, Monteiller V, Vanorio T, Got JL, Lyon-Caen H (2004) A new seismic tomography of Aigion area (Gulf of Corinth, Greece) from the 1991 data set. Geophys J Int 159(3):1013–1031

Lee WHK, Lahr JC (1972) HYPO71: a computer program for determining hypocenter, magnitude, and first motion pattern of local earthquakes, U.S. Geological Survey Open-File Report, pp. 100

McCarthy DD, Petit G (2004) IERS Conventions (2003), IERS TN32, Verlag des BKG, pp. 127

Okada Y (1992) Internal deformation due to shear and tensile faults in a half-space. Bull Seismol Soc Am 82:1018–1040

Paige CC, Saunders MA (1982) LSQR: an algorithm for sparse linear equations and sparse least squares.TOMS 8(1):43–71

Parsons T, Yeats RS, Yagi Y, Hussain A (2006) Static stress change from the 8 October, 2005 M=7.6 Kashmir earthquake. Geophys Res Lett 33. doi:10.1029/2005GL025429

Reasenberg PA (1985) Second-order moment of Central California Seismicity, 1969–1982. J Geophys Res 90:5479–5495

Reasenberg PA, Simpson RW (1992) Response of regional seismicity to the static stress change produced by the Loma Prieta earthquake. Science 255:1687–1690

Rietbrock A, Tiberi C, Sherbaum F, Lyon-Caen H (1996) Seismic slip on a low angle normal fault in the Gulf of Corinth: evidence from high resolution cluster analysis of microearthquakes. Geophys Res Lett 23(14):1817–1820

Rigo A, Lyon-Caen H, Armijo R, Deschamps A, Hatzfeld D, Makropoulos K, Papadimitriou P, Kassaras I (1996) A microseismic study in the western part of the Gulf of Corinth (Greece): Implications for large-scale normal faulting mechanisms. Geophys J Int 126:663–688

Roumelioti Z, Kiratzi A (2008) Moderate magnitude earthquake sequences in Central Greece (for the year 2008). Bull Geol Soc Greece XLIII(4):2144–2153

Schorlemmer D, Wiemer S, Wyss M (2005) Variation in earthquake-size distribution across different stress regimes. Nature 437:539–542

Sokos E, Zahradnik J, Kiratzi A, Jansky J, Gallovic F, Novotny O, Serpetsidaki A, Tselentis GA (2011) The January 2010 Efpalio earthquake sequence interpreted in terms of the tectonics of western Corinth Gulf. Geophys Res Abstr 13: EGU2011–EGU3032

Sokos E, Zahradník J, Kiratzi A, Janský J, Gallovič F, Novotny O, Kostelecký J, Serpetsidaki A, Tselentis G-A (2012) The January 2010 Efpalio earthquake sequence in the western Corinth Gulf (Greece). Tectonophysics 530–531:299–309

Taylor B, Weiss JR, Goodliffe AM et al (2011) The structures, stratigraphy and evolution of the Gulf of Corinth rift, Greece. Geophys J Int 185:1189–1219. doi:10.1111/j.1365-246X.2011.05014.x

Tselentis G-A, Zahradnik J (2000) The Athens earthquake of 7 September 1999. Bull Seismol Soc Am 90:1143–1160

Tsimi C, Ganas A, Soulakellis N, Kairis O, Valmis S (2007) Morphotectonics of the Psathopyrgos active fault, western Corinth rift, central Greece. Bull Geol Soc Greece 40:500–511

Vassilakis E, Royden L, Papanikolaou D (2011) Kinematic links between subduction along the Hellenic trench and extension in the Gulf of Corinth, Greece: A multidisciplinary analysis. Earth Planet Sci Lett 303:108–120. doi:10.1016/j.epsl.2010.12.054

Waldhauser F (2001) HypoDD: a computer program to compute double-difference earthquake locations, USGS Open File Report, 01-113

Wiemer S, Wyss M (2000) Minimum magnitude of completeness in earthquake catalogs: examples from Alaska, the western United States and Japan. Bull Seismol Soc Am 90:859–869

Wiemer S (2001) A software package to analyse seismicity: ZMAP. Seismol Res Lett 72(2):374–383

Wyss M, Pacchiani F, Deschamps A, Patau G (2008) Mean magnitude variations of earthquakes as a function of depth: Different crustal stress distribution depending on tectonic setting. Geophys Res Lett 35:L01307

Zelt BC, Taylor B, Sachpazi M, Hirn A (2005) Crustal velocity and Moho structure beneath the Gulf of Corinth, Greece. Geophys J Int 162:257–268